WELDING RESEARCH

SUPPLEMENT TO THE WELDING JOURNAL, SEPTEMBER, 1985

Sponsored by the American Welding Society and the Welding Research Council

Readers are advised that all papers published in the *Welding Journal's* Research Supplement undergo Peer Review before publication for: 1) originality of the contribution; 2) technical value to the welding community; 3) prior publication of the material being reviewed; 4) proper credit to others working in the same area; and 5) justification of the conclusions based on the results.

The names of the more than 160 individuals serving on the AWS Peer Review Panel are published periodically. All are experts in their respective technical areas, and all are volunteers in the program.

Surface Tension Gradient-Driven Flow Around an Electron Beam Welding Cavity

Surface tension as a function of temperature facilitates the flow of molten metal around EB cavity

BY P. S. WEI AND W. H. GIEDT

ABSTRACT. A two-dimensional model for the flow of molten metal in a thin layer around the central cavity formed during electron beam welding is proposed. This is based on vapor pressure supporting the cavity and the flow around it being driven by surface tension variation with temperature. Velocity and temperature distributions in the liquid layer were determined from a self-convergent finite difference procedure developed. Results for the liquid layer thickness and free surface temperature distributions are presented for appropriate ranges of surface tension number, Reynolds number, solid melting-conduction rate number and Peclet number. The dominant effect of surface tension gradient is demonstrated by noting that doubling of this variable with a constant Reynolds number decreases the local thickness of the liquid layer by about 20 percent compared to only a 6 percent decrease for a similar decrease in Reynolds number with a constant surface tension gradient.

Introduction

Electron beam (EB) welds are characterized by deep and narrow fusion zones. Surface width to depth ratios are typically 5 to 10 or greater (Ref. 1). These are achieved by directing a highly focused beam of high velocity electrons* on the interface region of the materials to be joined which is moved at constant velocity under the electron beam. The action of such a beam is to produce a cavity of the shape illustrated in Fig. 1. This is a quasi-steady state condition in which the cavity is considered to be stationary with the base material moving toward it at the constant welding velocity. As the base material reaches the electron beam location, it is melted and flows in a thin layer around a vapor supported cavity to the rear where it cools and solidifies. The driving force for the flow has been postulated to be due to the increase in surface tension as the free surface temperature decreases from the forward centerline around the cavity (Ref. 3).

High speed photographs of EB weld cavity openings and of the cross-sections of cavities as revealed by X-ray beams show that oscillations occur in the molten liquid flow, and that under some conditions these oscillations involve partial filling and opening of the cavity (Refs. 4-6). These oscillations depend on the particular material being welded and on welding conditions such as beam focus, power and welding speed. They generally follow a regular periodic pattern, but with some materials occur sporadically (Ref. 7).

It appears, however, that the quasi-steady interpretation of the EB welding process described above is a good average representation of the energy transfer

P. S. WEI is with the Department of Mechanical Engineering, National Sun Yat-Sen University, Kaohsiung, Taiwan. W. H. GIEDT is with the Department of Mechanical Engineering, University of California, Davis, Calif.

**Accelerating voltages range from 20 to 200 kV in current machines and focused beam energy fluxes are on the order of 10^6 W/cm^2 or greater (Ref. 2).*

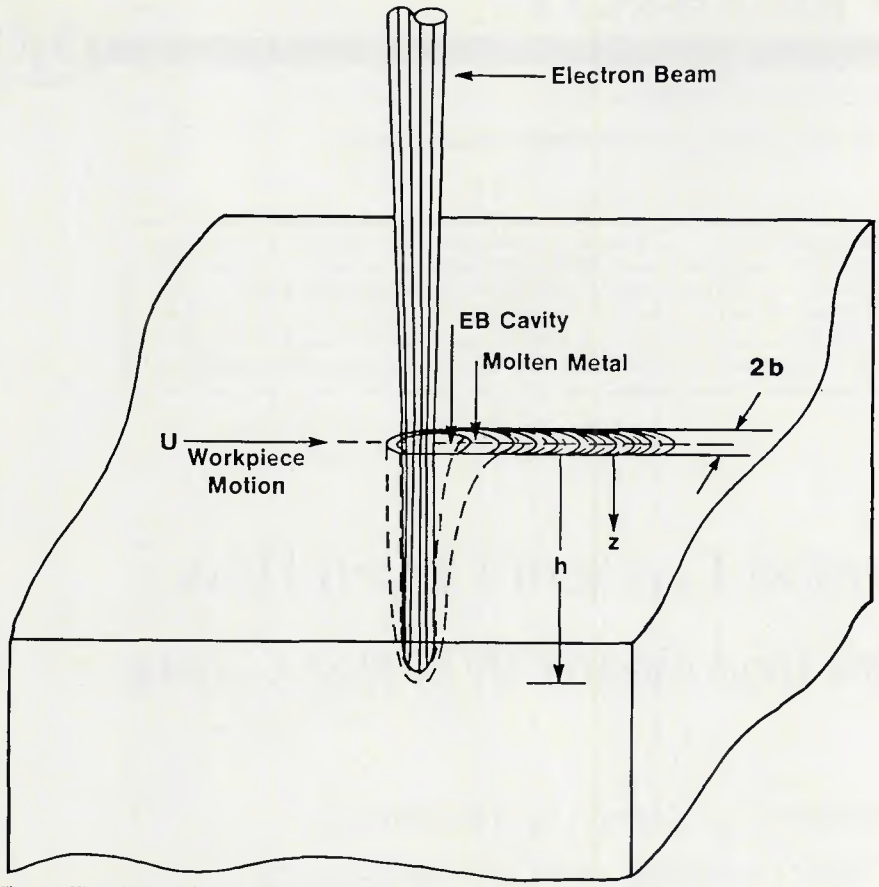

Fig. 1 — The electron beam welding process

and molten metal flow. This interpretation accounts for the deep welds which can be produced and has been used as the basis for successful predictions of weld penetration depth (Refs. 8, 9). The analyses in these references are based on determining the heat transfer into the base material surrounding the liquid layer from the solution for the temperature distribution in the base material around a moving circular or elliptically-shaped cylinder. Recognizing that this energy comes from the liquid layer flowing along the solid base material boundary suggests that the next step in an improved understanding of the fundamental nature of the EB welding process would be analysis of the flow and heat transfer in the liquid flowing around a cavity. This was the objective of the present study.

Because of the complexity of the process, attention has first been given to the forward half of the cavity. In an initial exploratory study (Ref. 10), limited results for one welding speed in aluminum were obtained using the local non-similarity boundary layer solution method. In addition to neglecting flow direction conduction, the numerical finite difference solution procedure involved visual computer terminal comparisons to determine trial and error changes.

A formal algorithm which removes these shortcomings was then developed. It is a self-convergent finite difference procedure for solving the governing equations in dimensionless form and was used to make a parametric study of the relative importance of surface tension gradient, welding speed and base material properties. This procedure is described in the following sections, and the results obtained for the liquid layer thickness and the free surface temperature distributions are illustrated.

Fluid Flow and Heat Transfer Model

Assumptions

For typical EB welds, where the ratio of the weld depth to the surface opening width (Fig. 1) is on the order of 5 to 10 or greater, conduction in the z direction in the surrounding base material is minimal. Assuming this and vertical flow to be negligible, the process at any representative horizontal plane can be approximated to be two-dimensional. This is implied in Fig. 2, which illustrates the flow around a forward quadrant of a cavity. The plane of the figure is normal to the beam axis. The elliptical shape of the solid-liquid interface is based on the weld region shape observed in high speed photographs. Assuming the thickness of the liquid layer to be small, relative to the cavity dimensions, it is then possible to select a coordinate system whose abscissa, x, is measured along the wall, and ordinate, y, is measured at right angles to it. This provides an orthogonal curvilinear net consisting of curves which are parallel to the wall and of straight lines perpendicular to the wall. The corresponding velocity components are denoted by u and v, respectively. For convenience, the stream function is specified to be zero from the weld centerline through the liquid layer and then along the free surface. Since the incoming velocity is constant, the stream function at any location along the solid-liquid interface must then simply be equal to $Ub \sin \theta$.

Since cavity widths are commonly around 0.3 cm (0.12 in.), it is believed that the vapor pressure is essentially uniform at any depth in a cavity (Ref. 3). An order of magnitude estimate (Ref. 11, Appendix II) of the velocity in the liquid layer indicates that the dynamic pressure is small and can be neglected. Therefore, the only driving force for causing the fluid to flow is postulated to be the change of the surface tension resulting from the temperature decreasing along the free surface of the cavity from the front to the side.*

The vertical slope of the forward wall of the cavity is very steep. Hence, electrons which reach the wall directly will have large incident angles. Most of these will be scattered after depositing some energy. Electrons which do penetrate the surface will be those which have been slowed by one or more interactions with the cavity surface. The penetration of the electron beam in the liquid layer can therefore be considered negligible, and heating by an electron beam can be assumed to be a surface source. Also, for this initial study, constant properties were assumed.

Governing Equations

With the above assumptions and estimated Reynolds and Peclet numbers on the order of 400 and 0.5, respectively, the applicable forms of the continuity,

**A temperature variation along the liquid surface would imply a variation of the vapor pressure, if the liquid and vapor were in local equilibrium. Hence, the assumption of a uniform vapor pressure at any depth in a cavity means that the liquid and vapor are not locally in equilibrium. The degree of nonequilibrium will be dependent on the local rates of evaporation and condensation. The possibility that this could produce some pressure variation in the liquid is recognized, and investigation of the effect is planned.*

momentum, and energy equations become

$$\frac{\partial u}{\partial x} + \frac{\partial v}{\partial y} = 0 \tag{1}$$

$$u\frac{\partial u}{\partial x} + v\frac{\partial u}{\partial y} = \nu\frac{\partial^2 u}{\partial y^2} \tag{2}$$

$$u\frac{\partial T}{\partial x} + v\frac{\partial T}{\partial y} = \alpha_\ell\left(\frac{\partial^2 T}{\partial x^2} + \frac{\partial^2 T}{\partial y^2}\right) \tag{3}$$

Boundary Conditions

At the solid-liquid interface (y = 0), the boundary conditions to be satisfied are

$$u = \frac{U\sin\theta}{\sqrt{\sin^2\theta + \left(\frac{b}{a}\right)^2\cos^2\theta}} \tag{4}$$

$$v = \frac{\left(\frac{b}{a}\right)U\cos\theta}{\sqrt{\sin^2\theta + \left(\frac{b}{a}\right)^2\cos^2\theta}} \tag{5}$$

$$T = T_{melt} = T_m \tag{6}$$

$$k_\ell\left(\frac{\partial T}{\partial y}\right)_{y^+=0} = k_s\left(\frac{\partial T}{\partial y}\right)_{y^-=0} + \frac{\left(\frac{b}{a}\right)\rho U h_{s\ell}\cos\theta}{\sqrt{\sin^2\theta + \left(\frac{b}{a}\right)^2\cos^2\theta}} \tag{7}$$

where $h_{s\ell}$ = heat of fusion of the workpiece. At the free surface y = δ(x)

$$\mu\left(\frac{\partial u}{\partial y}\right) = C_\sigma\left(\frac{\partial T}{\partial x}\right) \tag{8}$$

In equation (8), it has been assumed that the surface tension variation with temperature can be represented by $\sigma = \sigma_m + C_\sigma(T - T_m)$.
At the weld centerline where x = 0,

$$\frac{\partial T}{\partial x} = 0. \tag{9}$$

According to the results obtained in Ref. 10, the temperature gradient in the region of $\theta \sim 90°$ is essentially linear. Thus, the boundary condition at this location, which is denoted by x = L, is given by

$$T = T_m + \left(\frac{\partial T}{\partial y}\right)_{y^+=0} y \tag{10}$$

The heat flux at the solid-liquid interface specified by equation (7) is determined by conduction into the base material and the local fusion rate. The conduction loss into the base material can be determined from the solution for the temperature distribution around an elliptical cylinder at T_m moving through the base material at a constant speed (Ref. 9). Illustrative dimensionless heat rate distributions thus determined for an axis ratio of 1.5 are shown in Fig. 3 for a series of values of the parameter $A = Ub/2\alpha_s$ (when written as $U\rho_s c_{ps}/(2k_s/b)$, A can be seen to be a ratio of the rate of incoming base material energy to the conduction rate into the base material).

For the boundary condition at the free surface, the shear stress is balanced by the rate of change of the surface tension. Since the surface tension force distribution is determined by the free surface temperature distribution, the momentum and energy equation are coupled through equation (8). Unfortunately, neither the distribution of the free surface temperature nor the liquid layer thickness is known explicitly. Therefore, to begin the integration it is necessary to specify either the liquid layer thickness distribution or the free surface temperature distribution. This problem is thus classified as an inverse free surface problem (Ref. 12).

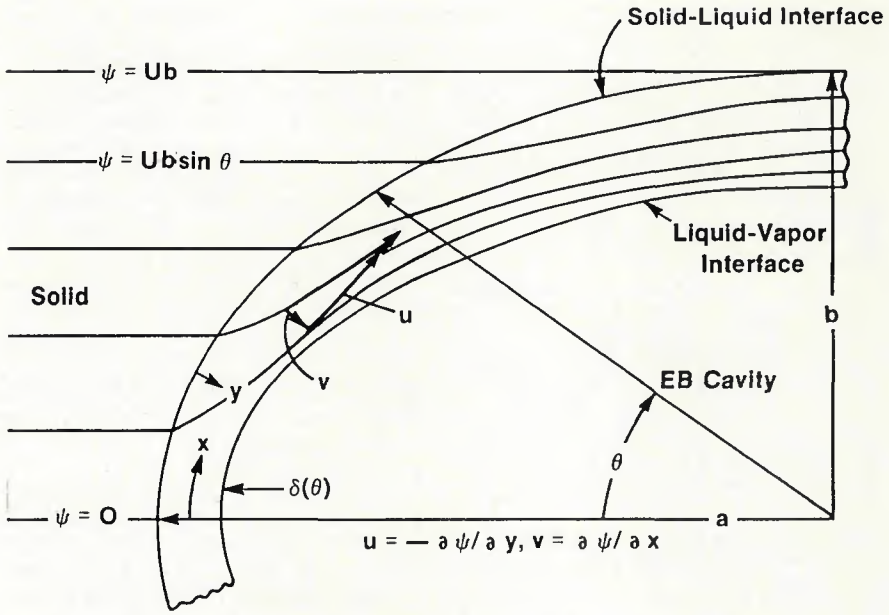

Fig. 2—Electron beam welding cavity liquid layer flow model and coordinate system

Self-Convergent Finite Difference Solution Procedure

Transformation of Flow Field to Rectangular Domain

Since this is a free surface problem, the domain of the flow field is unknown. A simple way to provide a rectangular mesh convenient for finite difference computations in this case is to introduce new dimensionless independent variables defined by $\xi = x/b$, and $\eta = y/\delta(\xi)$, where $\delta(\xi)$ is the unknown liquid layer thickness variation with ξ. The dimensionless stream function and the temperature distributions are defined as

$$\Psi = \psi/Ub$$

and $$\Phi = (T - T_m)/(T_m - T_\infty)$$

Here, the stream function is related to u and v according to $u = -\partial\psi/\partial y$ and $v = \partial\psi/\partial x$.

Governing Equations and Boundary Conditions

By introducing the stream function, the continuity equation (1) is automatically satisfied. Therefore, the governing equations (2), (3), and boundary conditions (4)-(10) become

$$\frac{\partial^3\Psi}{\partial\eta^3} - \mathrm{Re}\frac{d\Delta}{d\xi}\frac{\partial\Psi^2}{\partial\xi} + \mathrm{Re}\Delta\left(\frac{\partial^2\Psi}{\partial\xi\partial\eta}\frac{\partial\Psi}{\partial\eta} - \frac{\partial\Psi}{\partial\xi}\frac{\partial^2\Psi}{\partial\eta^2}\right) = 0 \tag{11}$$

$$\left[1 + \eta^2\left(\frac{d\Delta}{d\xi}\right)^2\right]\frac{\partial^2\Phi}{\partial\eta^2} + \Delta^2\frac{\partial^2\Phi}{\partial\xi^2} - 2\Delta\frac{d\Delta}{d\xi}\eta\frac{\partial^2\Phi}{\partial\xi\partial\eta} + \left[2\left(\frac{d\Delta}{d\xi}\right)^2 - \Delta\frac{d^2\Delta}{d\xi^2}\right]\eta\frac{\partial\Phi}{\partial\eta} - \Delta\mathrm{Pe}\left(\frac{\partial\Phi}{\partial\eta}\frac{\partial\Psi}{\partial\xi} - \frac{\partial\Psi}{\partial\eta}\frac{\partial\Phi}{\partial\xi}\right) = 0 \tag{12}$$

$$\frac{\partial \Psi}{\partial \eta}(\xi,0) =$$

$$\frac{-\Delta \sin \Theta}{\sqrt{\sin^2 \Theta + \left(\frac{b}{a}\right)^2 \cos^2 \Theta}} \quad (13)$$

$$\Psi(\xi,1) = 0 \quad (14)$$

$$\Psi(0,\eta) = 0 \quad (15)$$

$$\Phi(\xi,0) = 0 \quad (16)$$

$$\frac{\partial \Phi}{\partial \eta}(\xi,1) = \frac{\frac{\partial^2 \Psi}{\partial \eta^2}\sqrt{\left(\frac{d\Delta}{d\xi}\right)^2 + 1}}{S\Delta^2} \quad (17)$$

$$\frac{\partial \Phi}{\partial \eta}(\xi,0^+) = K\frac{\partial \Phi}{\partial \eta}(\xi,0^-) +$$

$$\frac{(F/R)\Delta \cos \Theta}{\sqrt{\sin^2 \Theta + \left(\frac{b}{a}\right)^2 \cos^2 \Theta}} \quad (18)$$

$$\Psi(\xi,0) = \sin \Theta \quad (19)$$

where the dimensionless parameters are defined as follows:

$$Re = \frac{Ub}{\nu} \quad (20)$$

$$S = \frac{C_\sigma(T_m - T_\infty)}{\mu U} \quad (21)$$

$$Pe = \frac{Ub}{\alpha_\ell} \quad (22)$$

$$K = \frac{k_s}{k_\ell} \quad (23)$$

$$F = \frac{\rho h_{s\ell} Ub}{k_\ell (T_m - T_\infty)} \quad (24)$$

$$R = \frac{a}{b} \quad (25)$$

$$\Delta = \frac{\delta(\xi)}{b} \quad (26)$$

$$A = \frac{Ub}{2\alpha_s} \quad (27)$$

The global boundary condition, equation (19), is obtained by integrating the mass of incoming solid material from the weld centerline to any location of Θ.

Solution Procedure

The finite difference representation chosen is similar to that of Keller's Box scheme (Ref. 13) in which partial differential equations are reduced to a system of first order partial differential equations. The central finite difference equations and the integration procedure are described in Ref. 11.

In the way in which the finite difference equations were formulated, the liquid layer thickness distribution and its first and second derivatives had to be known before the integration could be carried out. It is known that truncation errors and round-off errors always cause deterioration of the derivatives. Thus, specification of the second derivative of the liquid layer thickness distribution appeared appropriate. However, this will not yield the absolute thickness of the liquid layer. A technique which proved to be satisfactory was to specify the liquid layer thickness at several locations and then to approximate the distribution between these locations using the cubic spline method.

Optimization Procedure

The temperature distribution along the free surface can be determined in two different ways: one is from the integration of the surface tension boundary condition, equation (17); the other is from the solution of the finite difference computations. If the least squares variation of both distributions is less than a specified error limit, the solution is determined. The entire problem was thus reformulated in terms of the following optimization requirement:

Minimize

$$F(\Delta(\xi)) = [\Phi_s(\xi_1,1) - \Phi(\xi_1,1)]^2 + \ldots + [\Phi_s(\xi_N,1) - \Phi(\xi_N,1)]^2 \quad (28)$$

where the Φ's are calculated from the solution of the momentum and energy equations subject to the given boundary conditions, and the Φ_s's are calculated from integrating the surface tension boundary condition. The subscripts to ξ(*i.e.*, 1, . . . , N) denote the locations selected to specify one distribution of δ.

The solution of an inverse free surface problem is subject to instability. This necessitated the use of a constrained optimization technique to determine a distribution $\Delta(\xi)$ for specified welding conditions. A procedure which proved to be successful is a modification of the simplex method developed by Box (Ref. 14) and designated as a Complex optimization method. The key steps in the algorithm are the following:

1. Select (or specify) two liquid layer thickness distributions, within which all the liquid layer thickness distributions will fall. This can be done by assuming an average liquid velocity and satisfying continuity.

2. An original Complex of K = N+1 points (K points mean K distributions of the liquid layer thickness in this problem; each point represents one distribution of the liquid layer thickness and is defined by specifying δ at N locations of ξ) is then developed consisting of the two specified in step 1 and N−1 additional points generated by applying the following relation:

$$\Delta_i(\xi_j) = G(\xi_j) + R_{i,j}\ [H(\xi_j) - G(\xi_j)], \quad i = 1, \ldots, N-1\ j = 1, \ldots, N$$

where $R_{i,j}$ are random numbers between 0 and 1 and $G(\xi_j)$ and $H(\xi_j)$ are the values of Δ specified in step 1 at the N locations of ξ.

3. All selected or calculated points must satisfy the specified constraints. If at any time the constraints are violated, the point is changed so that it falls just inside the violated limit.

4. The objective function (equation (28)) is evaluated at each point, *i.e.*, for each of the K distributions of liquid layer thickness. The point having the largest function value (denoted by $\Delta_r(\xi j)$) is replaced by a point which is located at a distance from the centroid of the remaining points equal to β times the distance between the rejected point and the centroid; *i.e.*,

$$\Delta_{new}(\xi_j) = \beta[\Delta_c(\xi_j) - \Delta_r(\xi_j)] + \Delta_c(\xi_j), \quad j = 1, \ldots, N$$

where $\Delta_c(\xi_j) = \sum_{i=1}^{K-1} [\Delta_i(\xi_j) - \Delta_r(\xi_j)]/(K-1)$, $i \neq r$, $j = 1, \ldots, N$

Box recommends a value of $\beta = 1.3$.

5. If a point repeats in giving the largest function value on consecutive tri-

Table 1—Ranges of Dimensionless Parameters

	Dimensionless Parameters		
Materials	A	F	K
Al	0.05 to 0.20	0.12 to 0.50	2.5
Fe	0.50 to 1.40	0.18 to 0.55	0.84
ST	0.90 to 1.80	0.40 to 0.80	0.70
	Pe	Re	R
Al	0.20 to 0.79	10.0 to 40.8	1.5 to 2.0
Fe	0.82 to 2.50	7.0 to 21.0	1.5 to 2.0
ST	1.27 to 2.54	8.0 to 16.0	1.5 to 2.0
	S		
Al	−5560 to −16000		
Fe	−8000 to −16800		
ST	−5190 to −10370		

als, it is moved one half the distance toward the centroid of the remaining points.

6. The new point is checked against the constraints and is adjusted as before if the constraints are violated.

7. Repeat steps 4 to 6 until the objective function value for one of the N+1 distribution of $\Delta(\xi)$ is less than a specified minimum value (4×10^{-4} in the present study).

Significant Ranges of Dimensionless Variables

The governing parameters arising in the non-dimensionalized equations and boundary conditions are a Reynolds number, Re, Peclet number, Pe, surface tension number, S, fusion energy ratio, F, conductivity ratio, K, ellipse axis ratio, R, describing the shape of the cavity, and a parameter A which is the ratio of the incoming solid sensible energy rate to the conduction rate in the solid. These are defined by equations (20)-(27).

The ranges of the above dimensionless parameters relevant to electron beam welding are listed in Table 1. These values are based on the thermal properties and welding speeds normally used for aluminum, iron, and steel.

Results and Discussion

Before applying the self-convergent finite difference procedure developed to investigate the fluid flow and heat transfer in the liquid layer in an EB cavity, consideration was given to the relative importance of the seven dimensionless parameters listed in the previous section. The viscous force, the surface tension force, and the inertia force are the forces which control the fluid flow around the cavity. Hence, an understanding of the effects of changes in the Reynolds number and the surface tension number on the fluid flow are of primary importance. From high speed photographs of electron beam welding of different materials, the axis ratio is observed to be around 1.5. This mean value was therefore chosen for the calculations. Although the ratio of the highest to the lowest value of Peclet number in Table 1 is on the order of 10, the range of values listed is small (0.2 to 2.54). Changes over this range are expected to be small, so a mean value of Pe = 1.2 was selected for most of the cases considered. The ratio of the fusion energy rate to the conduction rate in the liquid at the solid-liquid interface is on the order of $(\rho_s U h_{s\ell})(k_\ell\ \Delta T/\delta)$. Since ΔT is around 100°C (180°F) for Al and 300°C (540°F) for iron, the fusion energy ratio is on the order of 0.1 for aluminum (with U ~ 1.2 cm/s (0.47 in./s)) and 0.2 for iron (with U ~ 0.9 cm/s (0.35 in./s)). This indicates that the effect of the energy rate required for fusion will not be of major importance. The temperature distribution in the liquid layer will, however, be strongly influenced by the change in heat transfer at the liquid-solid interface as indicated by the curves in Fig. 3 for different values of the parameter A. These considerations lead to selection of the values of the dimensionless parameters listed in Table 2 for calculations.

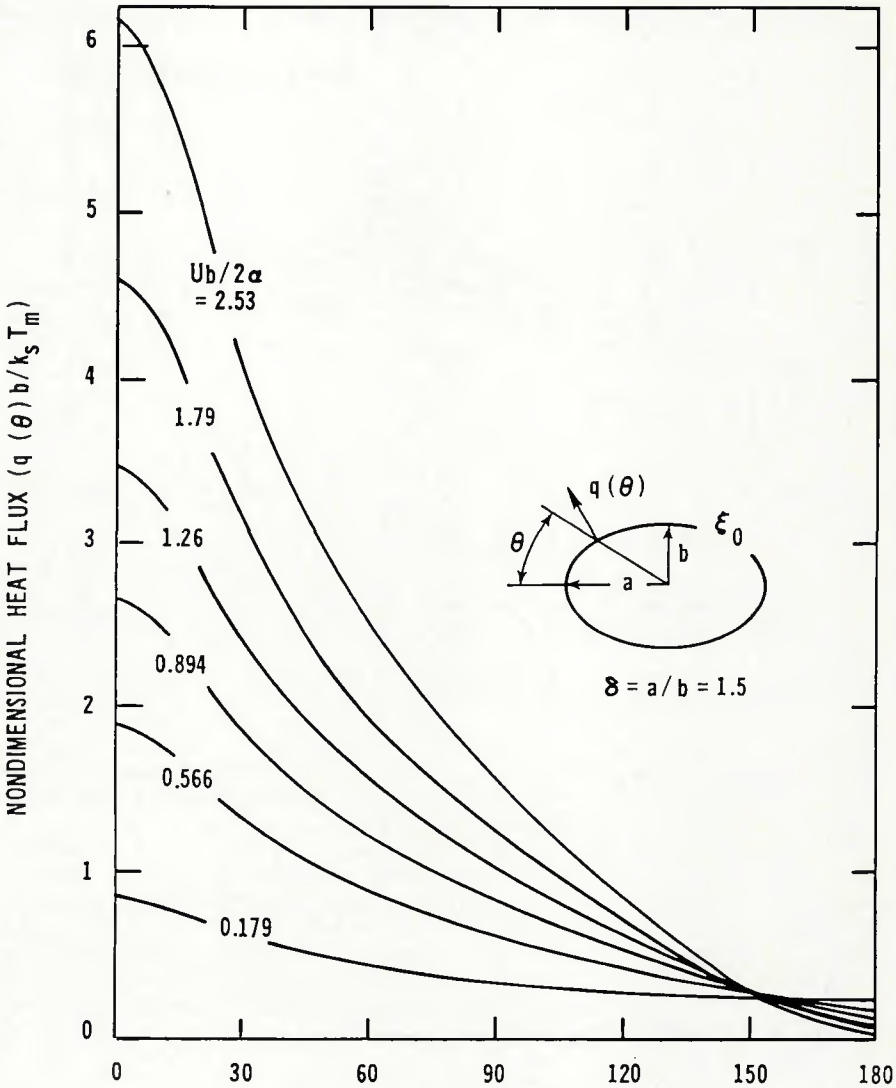

Fig. 3—Dimensionless temperature gradients at solid boundary

Liquid Layer Thickness Distribution

The variation in liquid layer thickness

Table 2—The Values of Dimensionless Parameters Selected for Calculations

Case	Re	S	A	Pe	K	F	R
1	10	−10,000	0.9	1.2	1.5	0.5	1.5
2	20	−10,000	0.9	1.2	1.5	0.5	1.5
3	40	−10,000	0.9	1.2	1.5	0.5	1.5
4	20	−5000	0.9	1.2	1.5	0.5	1.5
5	20	−10,000	0.9	1.2	1.5	0.5	1.5
6	20	−20,000	0.9	1.2	1.5	0.5	1.5
7	20	−10,000	0.9	1.2	1.5	0.5	1.5
8	20	−10,000	1.26	1.2	1.5	0.5	1.5
9	20	−10,000	1.8	1.2	1.5	0.5	1.5
10	36.4	−6208	0.18	0.71	2.5	0.45	1.5
11	15.8	−5393	1.79	2.5	0.7	0.78	1.5

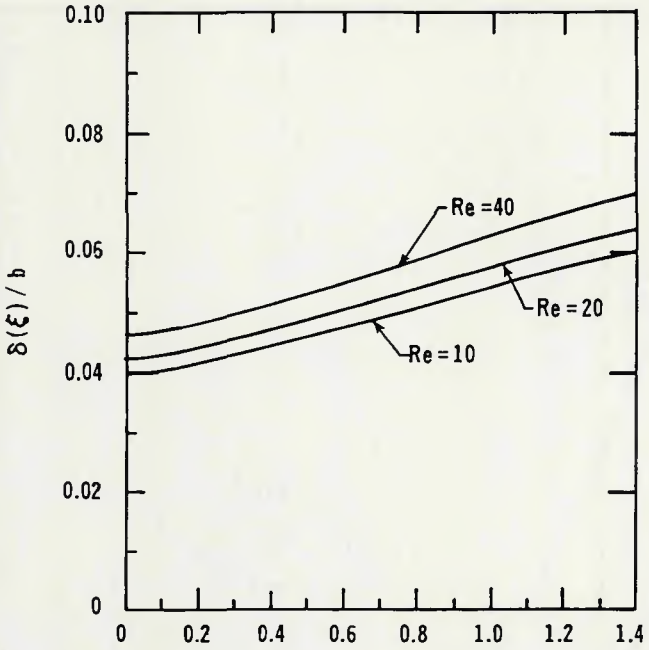

Fig. 4 – Variation of liquid layer thickness distribution with Reynolds number (S = −10,000, A = 0.9, Pe = 1.2, K = 1.5, F = 0.5, R = 1.5)

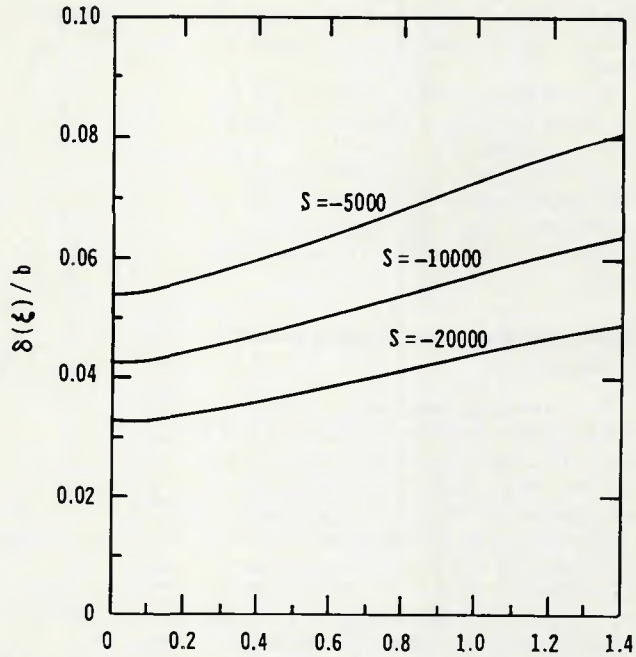

Fig. 5 – Variation of liquid layer thickness distribution with surface tension number (Re = 20, A = 0.9, Pe = 1.2, K = 1.5, F = 0.5, R = 1.5)

distribution for Reynolds numbers of 10, 20, and 40 is shown in Fig. 4 for mean values of the other dimensionless parameters (viz., S = −10,000, A = 0.9, Pe = 1.2, K = 1.5, F = 0.5, R = 1.5). In general, the thickness increases by about 50%, from $\xi = 0$ to $\xi = 1.4$ (which corresponds to an angle of about 70° for R = 1.5). Also, as can be noted, increasing the Reynolds number increases the thickness but has little effect on the shape of the distribution. The increase in thickness is almost linear over the range investigated.

Referring to Fig. 5, it can be seen that surface tension has a greater effect on the liquid layer thickness than the Reynolds number. On the average, doubling the surface tension number causes the liquid layer thickness to decrease by 20 percent, whereas a similar decrease in Reynolds number results in only a 6 percent decrease – Fig. 4. This is indicative of the strong influence which the change in surface tension with temperature can have on fluid flow.

For Cases 7-9, the Reynolds and surface tension numbers were held constant and A varied from 0.9 to 1.8. These conditions imply similar welding speeds with different materials of which the thermal diffusivity, α_s, decreases (thus increasing A). The effect of such a change

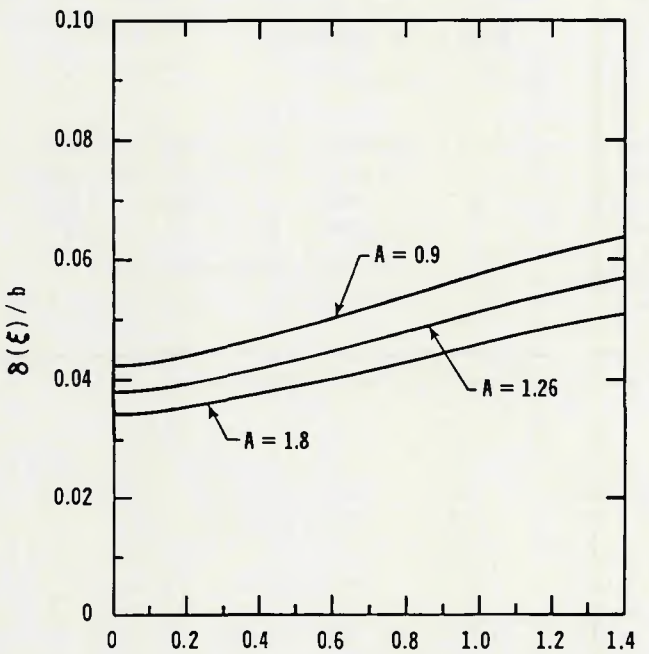

Fig. 6 – Variation of liquid layer thickness distribution with solid convection-conduction number A (Re = 20, S = −10,000, Pe = 1.2, K = 1.5, F = 0.5, R = 1.5)

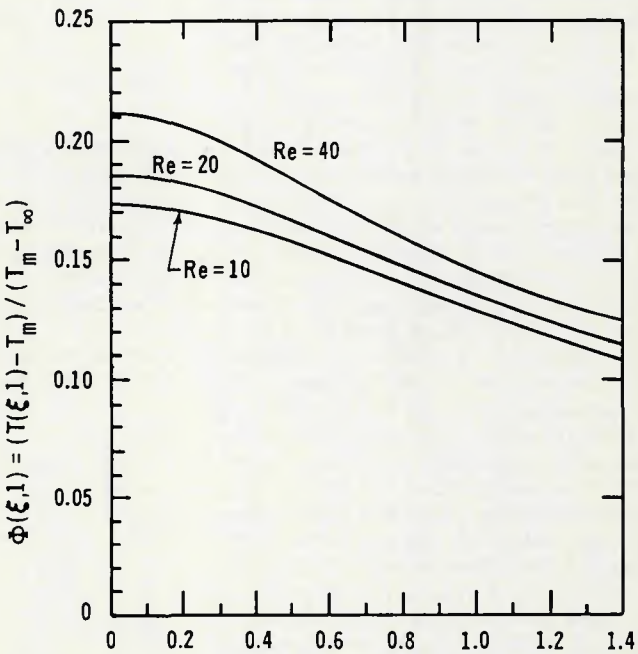

Fig. 7 – Variation of free surface temperature distribution with Reynolds number (S = −10,000, A = 0.9, Pe = 1.2, K = 1.5, F = 0.5, R = 1.5)

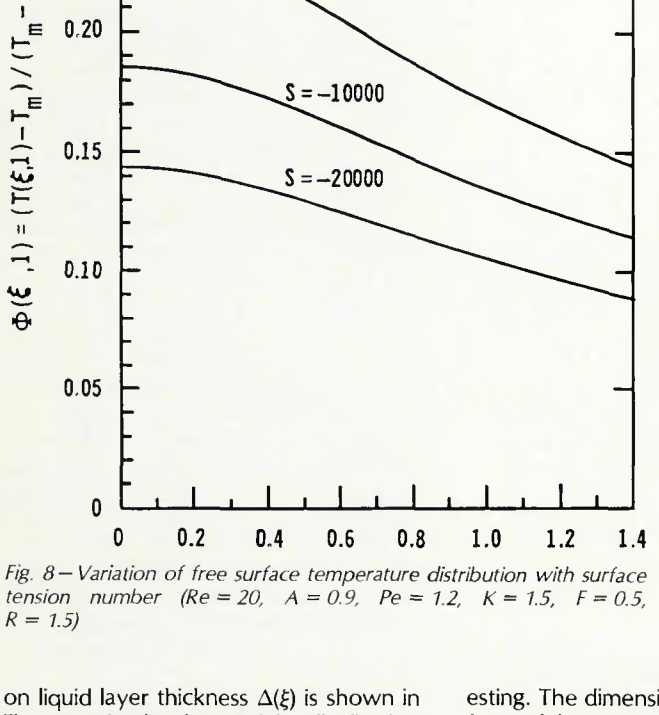

Fig. 8 — Variation of free surface temperature distribution with surface tension number (Re = 20, A = 0.9, Pe = 1.2, K = 1.5, F = 0.5, R = 1.5)

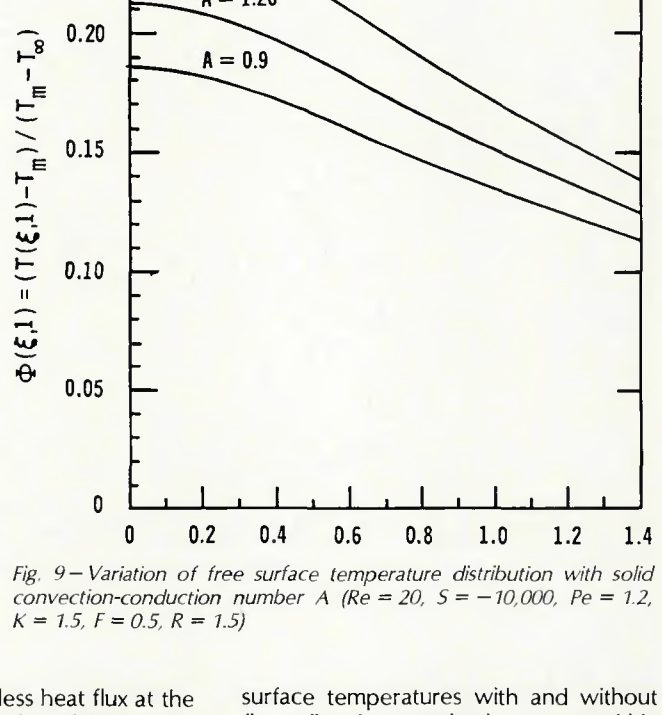

Fig. 9 — Variation of free surface temperature distribution with solid convection-conduction number A (Re = 20, S = −10,000, Pe = 1.2, K = 1.5, F = 0.5, R = 1.5)

on liquid layer thickness $\Delta(\xi)$ is shown in Fig. 6. Again, the shape of the distribution is not significantly affected, which is somewhat surprising in that the distributions of the conduction rate into the base material increase rapidly for low values of ξ with increasing A. The resulting more rapid decrease in the conduction heat flux into the base material causes the free surface temperature to decrease more rapidly for larger A, which produces a stronger surface tension force. The liquid layer thickness therefore decreases.

Free Surface Temperature Distribution

Turning now to the free surface temperature distribution, the effect of increasing the Reynolds number as shown in Fig. 7 is to increase the magnitude of the temperature. The increase is greater in the range of $0 < \xi < 0.5$ than for $\xi > 0.5$. This is attributable to the very rapid decrease of the heat flux into the solid from $\xi = 0$ to $\xi = 0.5$ (Fig. 3) and the higher fusion energy rate in this region.

Figure 8 shows the variation of the free surface temperature distribution with the surface tension number. Similar to the liquid layer thickness, the influence of the surface tension number on the free surface temperature is stronger than that of the Reynolds number. The free surface temperature (referenced to the melting temperature) decreases about 20 percent with a doubling of the surface tension number.

The variation of the free surface temperature with A shown in Fig. 9 is interesting. The dimensionless heat flux at the front of the cavity into the solid is around 2.6 for A = 0.9 and increases to 3.5 at A = 1.26 — Fig. 3. This results in a higher liquid surface temperature, even though the liquid layer thickness decreases as A increases — Fig. 6.

Effect of Conduction in Flow Direction

To investigate the influence of conduction in the flow direction, calculations were made for typical welding conditions in aluminum (for which the Peclet number is around 0.71) and for steel (for which the Peclet number is around 2.5). These are listed as cases 10 and 11 in Table 2. In order to evaluate the conduction effect in the flow direction, the finite difference equations in the computer program were modified by deleting the terms which represented the second derivative of the temperature with respect to the flow direction. Results were first computed with the complete computer program and then with the modified program.

Comparison of the results obtained for Pe = 0.71 showed that when conduction is included, the liquid layer thickness was around 2.5 percent greater than when conduction is neglected. A similar difference occurred in the values of the dimensionless surface temperature. Although these effects are relatively small, the slightly larger liquid thickness means lower velocities. The resulting reduced flow direction convection would be compensated for by the conduction. For Pe = 2.5, liquid layer thicknesses and free surface temperatures with and without flow direction conduction were within 0.5 percent or less, which is of the order of the accuracy of the numerical calculations. These results indicate that conduction in the flow direction is relatively unimportant.

Liquid Layer Characteristics for Iron

To illustrate actual magnitudes of the liquid layer characteristics predicted by the analysis presented, distributions of the free surface temperature, liquid layer thickness, and the velocity and temperature distributions through the layer are presented in Figs. 10, 11 and 12 for welding in iron. The values are shown in terms of the angle θ measured from the forward center of the weld and were determined from the non-dimensional results for case No. 11 in Table 2. This required selection of applicable values for the thermal and fluid-flow properties and the welding speed. One reason iron was chosen is that more material property data over the range of temperatures occurring during welding are available.

Recent measurements (Refs. 15, 16) show that the surface tension of iron decreases linearly with temperature above the melting point, as assumed in the analysis. Based on reported values of -0.38×10^{-3} and -0.41×10^{-3} N/m°C, C_σ (equation (8)) was taken as -0.40×10^{-3} N/m°C. Thermal conductivities and diffusivities (Refs. 17, 18) were: $k_s = 24.7$ and $k_\ell = 35.1$ W/m°C; $\alpha_s = 0.05 \times 10^{-4}$ and $\alpha_\ell = 0.072 \times 10^{-4}$ m²/s. With $T_\infty = 25$°C (77°F), and

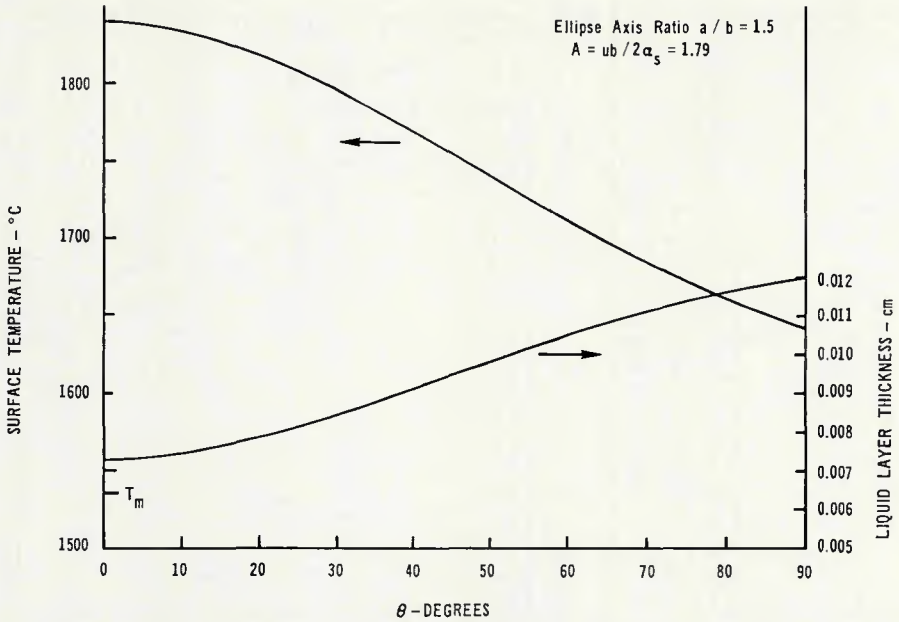

Fig. 10—Free surface temperature and liquid layer thickness distribution for welding iron with U = 1.2 cm/s

T_m = 1535°C (2795°F), $T_m - T$ = 1510°C (2718°F). For the viscosity μ, an average value of 0.009 Ns/m^2 was selected (Ref. 19). The heat of fusion $h_{s\ell}$ = 270 J/kg. Assuming a welding speed U = 0.72 m/min (28.4 in./min) then yields Re = 15.8, S = −5593, A = 1.79 and Pe = 2.5.

Note that (Fig. 10) the free surface temperature decreases from a maximum of 1840°C (3344°F) at $\theta = 0°$ to about 1650°C (3002°F) as $\theta \rightarrow$ 80–90°. Over the same range, the liquid layer thickness increases from about 0.0073 cm (0.003 in.) to around 0.012 cm (0.005 in.). Such a thin layer is indicative of the effectiveness of the surface tension gradient force. Distributions of the tangential velocities developed have been plotted in Fig. 11. The surface velocity increases from 0 at $\theta = 0°$ to about 10 cm/s at $\theta = 10°$. It continues to increase but less rapidly and reaches a maximum of about 29 cm/s around $\theta = 60°$. It decreases after this due to the decrease in the temperature gradient and the increased liquid layer thickness.

These results appear to be very reasonable for locations near a cavity opening or for a full penetration weld where the cavity opening is essentially uniform with depth. However, measurements in cavities in steel indicate that the surface temperatures increase to around 2200–2300°C (3992–4172°F) at the base (Ref. 20). Since the cavity size decreases with depth, the peak heat flux (Fig. 3) would also decrease. Higher surface temperatures near the base, thus, imply that the liquid layers are thicker in this region and that there is a downward component in the liquid flow.

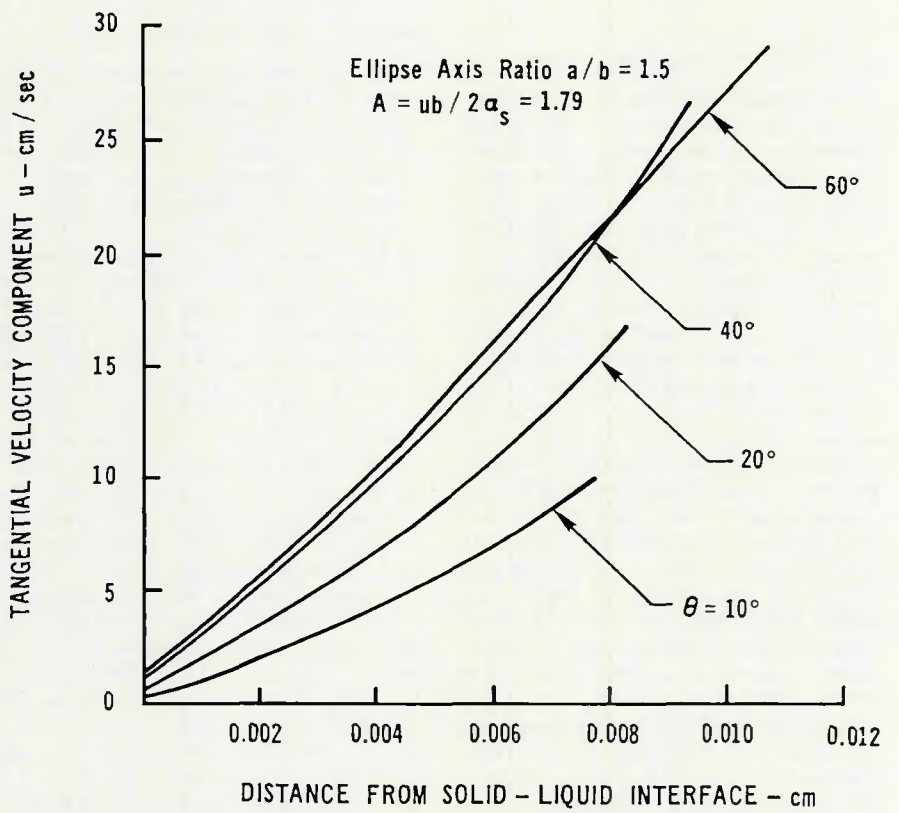

Fig. 11—Tangential velocity distributions in EB weld liquid layer (U = 1.2 cm/s in iron)

Conclusion

The results of this investigation clearly demonstrate that the variation of surface tension with temperature can provide the driving force for the movement of metal melted at the front of an EB cavity to the rear. In fact, it is found that for representative values of the surface tension gradient, predicted free surface velocities are on the order of tens of cm/s and the resulting liquid layers on the forward half of a cavity are only fractions of a millimeter thick. The important influence of fluid friction, however, is illustrated by noting that doubling the surface tension temperature gradient only changes the liquid layer thickness by around 20 percent.

Recalling that the penetration of electrons in metal is on the order of fractions of a millimeter suggests that the electron beam energy may well be deposited throughout the liquid layer rather than primarily at the surface as assumed in the analysis. This is not considered to be a serious point, however, because of the high thermal conductivity of the liquid metal. Although the magnitude of the temperature changes from the forward centerline to the side is not large (~ 50–100°C) (~ 90–180°F) compared to melting temperatures, the equilibrium vapor pressure does vary over this range. This could be a driving force when the surface tension decreases very slowly with temperature or even increases with

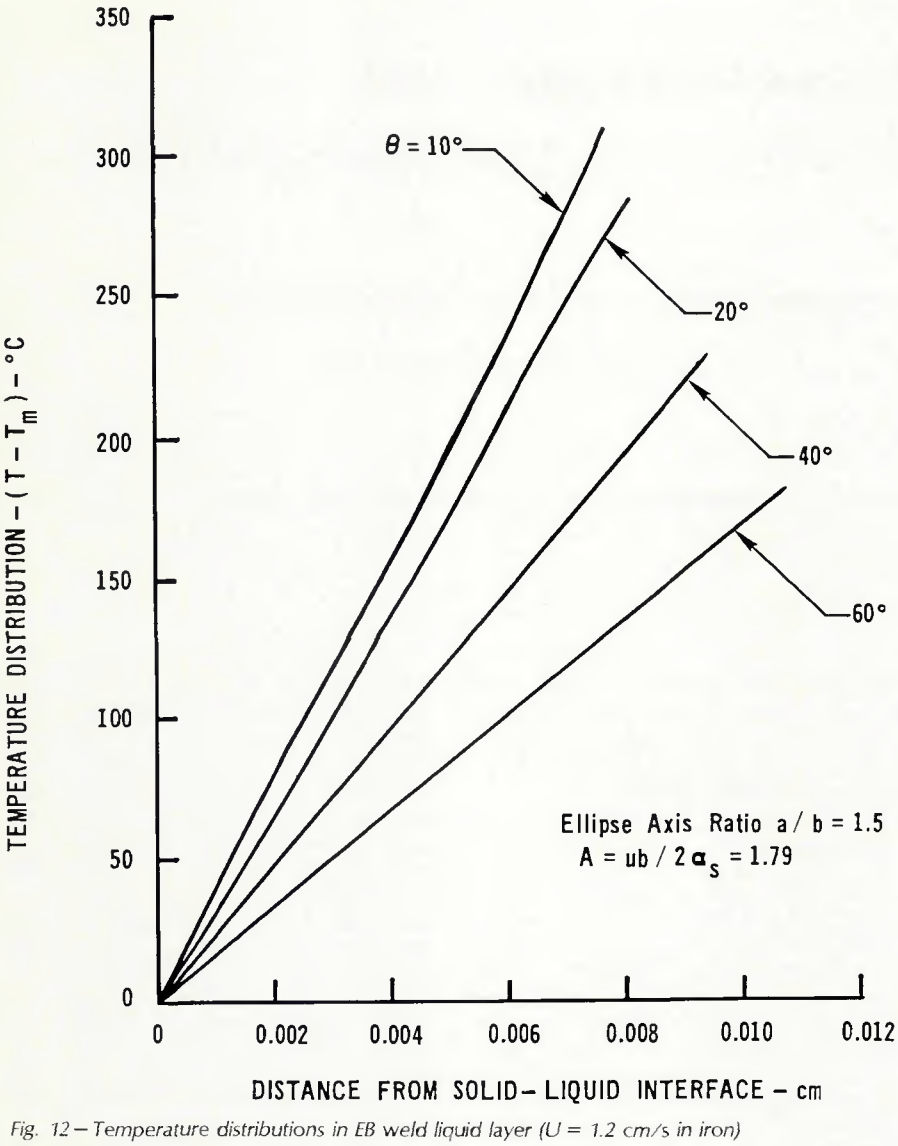

Fig. 12 – Temperature distributions in EB weld liquid layer (U = 1.2 cm/s in iron)

temperature. Hence, investigation of the possible magnitude and effect of pressure variation should now be considered.

Acknowledgment

The initial support of this study by the National Science Foundation under Grant No. CME-7911288 is gratefully acknowledged.

References

1. Kearns, W. H., ed., 1980. *Welding Handbook.* Am. Weld. Soc., Miami, Florida 3:169–215.

2. Bakish, R., and White, S. S. 1964. *Handbook of Electron Beam Welding.* John Wiley and Sons, New York.

3. Ol'shanskii, N. A. 1974. Movement of molten metal during electron beam welding. *Welding Production* 21:25–31.

4. Tong, H., and Giedt, W. H. 1969. Radiographs of the electron beam welding cavity. *Review of Scientific Instruments* 40:1283–85.

5. Tong, H., and Giedt, W. H. 1970. A dynamic interpretation of electron beam welding. *Welding Journal* 49(6):259-s to 266-s.

6. Kennish, W. J. 1972. Radiographic study of cavity fluctuation. Interagency Mechanical Operations Group, Vol. II, Electron Beam Welding Research, Jan. Rept. No. SC-DR-72-0637, Sandia Labs, Livermore, Calif.

7. Schauer, D. A., and Giedt, W. H. 1978. Prediction of electron-beam welding spiking tendency. *Welding Journal* 57(7):189-s to 195-s.

8. Tong, H., and Giedt, W. H. 1971. Depth of penetration during electron beam welding. *Trans. ASME, J. Heat Transfer* 93: Series C, pp. 155–63.

9. Miyazaki, T., and Giedt, W. H. 1982. Heat transfer from an elliptical cylinder moving through an infinite plate applied to electron beam welding. *Inter. J. of Heat and Mass Transfer* 25:807–14.

10. Giedt, W. H., and Wei, P. S. 1982. Temperature and velocity distributions in the liquid flowing around the front of an electron beam welding cavity. *Proc. of the Seventh Intl. Heat Transfer Conf.*, Hemisphere Publ. Corp., Washington, D.C., 6:403-407.

11. Wei, P. S. 1984. *Analysis of Velocity and Temperature Distributions in the Liquid Flowing around the Front of an Electron Beam Cavity.* Ph.D. Dissertation, University of California, Davis.

12. Glaswell, I., and Wait, R. 1979. *A Survey of Numerical Methods for Partial Differential Equations,* Clarendon Press, Oxford, pp. 310-56.

13. Keller, H. B. 1970. *A New Difference Scheme for Parabolic Problems, Numerical Solutions of Partial Differential Equations, II,* J. Bramble (ed.), Academic Press, New York, 1970.

14. Box, M. J. 1965. A new method of constrained optimization and a comparison with other methods. *Computer J.* 8:42–52.

15. Keene, B. J., Mills, K. C., et al. 1981. Effects of interaction between surface active elements on the surface tension of iron. *Canadian Metallurgical Quarterly* 21:393–403.

16. Kasama, A., McLean, A., et al. 1983. Surface tension of liquid iron and iron-oxygen alloys. *Canadian Metallurgical Quarterly* 22:9–17.

17. Touloukian, Y. S., Powell, R. W., et al. 1970. *Thermal Conductivity,* IFI/Plenum, New York.

18. Touloukian, Y. S., Powell, R. W., et al. 1973. *Thermal Diffusivity,* IFI/Plenum, New York.

19. Smithells, C. J., ed., 1976. *Metals Reference Book,* 5th ed., Butterworths, London, pp. 944–947.

20. Schauer, D. A., Giedt, W. H., and Shintaku, S. M. 1978. Electron beam welding cavity temperature distributions in pure metals and alloys. *Welding Journal* 57(5):127-s to 133-s.